ChemComm

COMMUNICATION

View Article Online
View Journal | View Issue

Cite this: *Chem. Commun.*, 2020, **56**, 9449

Received 11th May 2020,
Accepted 10th July 2020

DOI: 10.1039/d0cc03385e

rsc.li/chemcomm

Nucleophilic reactivity of a mononuclear cobalt(III)–bis(*tert*-butylperoxo) complex†

Bongki Shin, ‡ Younwoo Park,‡ Donghyun Jeong and Jaeheung Cho *

A mononuclear cobalt(III)–bis(*tert*-butylperoxo) adduct (Co^{III}–$(OO^tBu)_2$) bearing a tetraazamacrocyclic ligand was synthesized and characterized using various physicochemical methods, such as X-ray, UV-vis, ESI-MS, EPR, and NMR analyses. The crystal structure of the Co^{III}–$(OO^tBu)_2$ complex clearly showed that two OO^tBu ligands bound to the equatorial position of the cobalt(III) center. Kinetic studies and product analyses indicate that the Co^{III}–$(OO^tBu)_2$ intermediate exhibits nucleophilic oxidative reactivity toward external organic substrates.

Transition metal–alkylperoxo (M–OOR) species play an important role in oxidation reactions such as industrial and biological catalytic oxidation.[1–6] In industrial processes, M–OOR intermediates, such as Co^{III}–OOR complexes, were proposed as key intermediates in hydrocarbon catalytic oxidation under harsh conditions.[1,7] Mononuclear nonheme M–OOR complexes have been suggested to play a significant role in the oxidation reaction of metalloenzyme systems (*e.g.*, lipoxygenase and homoprotocatechuate 2,3-dioxygenase).[8,9] Biomimetic studies of M–OOR complexes enabled catalysts to be developed that produce high value-added organic products under mild conditions.

Mononuclear heme and nonheme first-row M–OOR intermediates (M = Mn, Fe, Co, Ni, and Cu) have been investigated as model complexes for the active sites of metalloenzymes.[2,5,6,10–13] A number of M–OOR complexes were mainly studied in the investigation of electrophilic reactions (*e.g.*, oxygen and hydrogen atom transfer reaction).[14–25] It has been reported that the reaction proceeds *via* the $^{\bullet}OOR$ and $^{\bullet}OR$ radicals from decomposition of the M–OOR species.[1] However, only a few examples of nucleophilic reactivity with M–OOR intermediates (M = Fe, Ni, and Cu) have been reported.[19,20,23]

In the Sharpless–Katsuki epoxidation, Ti–$(OOR)_n$ (n = 1–4) species were proposed as reactive intermediates.[26,27] Furthermore, in the formation of Fe–OO^tBu complexes, Fe–$(OO^tBu)_2$ species, $[Fe^{III}(TPP)(OO^tBu)_2]^-$ (TPP = 5,10,15,20-tetraphenylporphyrinate) and $[Fe^{III}(BPMCN)(OO^tBu)(HOO^tBu)]^{2+}$ (BPMCN = *N*,*N*′-bis(2-pyridylmethyl-*N*,*N*′-dimethyl-*trans*-1,2-diaminocyclohexane)) adducts, have been proposed as short-lived intermediates.[28–31] However, definitive evidence of bis(alkylperoxo) binding first-row transition metal compounds has not been reported yet. In this work, we report a fully characterized Co^{III}–$(OO^tBu)_2$ complex bearing a tetraazamacrocyclic ligand, $[Co^{III}(Me_3\text{-TPADP})(OO^tBu)_2]^+$ (**2**, Me_3-TPADP = 3,6,9-trimethyl-3,6,9-triaza-1(2,6)-pyridinacyclodecaphane). Intermediate **2** was investigated in nucleophilic reactions such as aldehyde oxidation. Only one of the two OO^tBu ligands in **2** is able to oxidize external substrates. In order to compare the structure and the reactivity of an alkylperoxo and bis(alkylperoxo) binding cobalt species, Co^{III}–$(OO^tBu)(X)$ complexes, $[Co^{III}(Me_3\text{-TPADP})(OO^tBu)(X)]^+$ (X = N_3 for **4**, NCS for **5**), were prepared as well.

The cobalt(II) starting complex, $[Co^{II}(Me_3\text{-TPADP})(CH_3CN)_2]^{2+}$ (**1**), was synthesized by using a published method.[32] When 10 equiv. of *tert*-butyl hydroperoxide (^tBuOOH) was added to **1** in the presence of 2 equiv. of triethylamine (TEA) in CH_3CN at 25 °C, the Co^{III}–$(OO^tBu)_2$ adduct, $[Co^{III}(Me_3\text{-TPADP})(OO^tBu)_2]^+$ (**2**), was generated and the solution color changed from purple to dark green (Scheme S1, ESI†). Intermediate **2** is thermally metastable in CH_3CN at 25 °C, which allowed us to use it for characterization and reactivity studies.

The UV-vis spectrum of **2** in CH_3CN at 25 °C shows electronic absorption bands at λ_{max} = ~360 (ε = 1100 M^{-1} cm^{-1}) and 583 nm (ε = 190 M^{-1} cm^{-1}) (Fig. 1a). Electrospray ionization mass spectrometry (ESI-MS) analysis of **2** exhibits a prominent ion peak at m/z 485.3, whose mass and isotope distribution pattern correspond to $[Co^{III}(Me_3\text{-TPADP})(OO^tBu)_2]^+$ (calcd m/z 485.3) (Fig. 1b). The X-band electron paramagnetic resonance (EPR) silence (Fig. 1a, inset) and ^1H NMR spectral features (Fig. S1, ESI†) in the diamagnetic region confirm that complex **2** is a low-spin S = 0 cobalt(III) species.

Department of Emerging Materials Science, DGIST, Daegu 42988, Korea. E-mail: jaeheung@dgist.ar.kr

† Electronic supplementary information (ESI) available: Synthesis and characterization data and kinetic details. CCDC 1906994–1906996. For ESI and crystallographic data in CIF or other electronic format see DOI: 10.1039/d0cc03385e

‡ These authors contributed equally to this work.

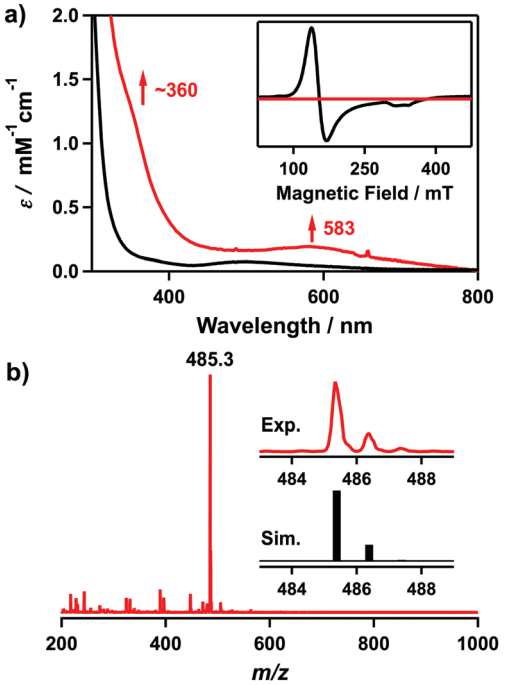

Fig. 1 (a) UV-vis spectra of $[Co^{II}(Me_3\text{-TPADP})(CH_3CN)_2]^{2+}$ (**1**) (the black line) and $[Co^{III}(Me_3\text{-TPADP})(OO^tBu)_2]^+$ (**2**) (the red line) in CH_3CN at 25 °C.[32] Inset shows the X-band EPR spectra of **1** (the black line) in frozen CH_3CN at 5 K and **2** (the red line) in frozen CH_3CN at 113 K.[32] The parameters for the measurement of **2**: microwave power = 1.0 mW, frequency = 9.176 GHz, sweep width = 0.40 T, and modulation amplitude = 0.60 mT. (b) ESI-MS of **2** in CH_3CN at −40 °C. Insets show experimental (upper) and simulated (lower) isotope distribution patterns.

The X-ray crystal structure of $[Co^{III}(Me_3\text{-TPADP})(OO^tBu)_2](BPh_4)(Et_2O)$ (**2**-$BPh_4{\cdot}Et_2O$) revealed a distorted octahedral geometry where two *tert*-butyl peroxide ligands coordinate to the cobalt(III) center in the *cis* positions (Fig. 2a). To the best of our knowledge, this is the first crystal structure of a mononuclear Co^{III}–$(OO^tBu)_2$ complex. The average Co–O (1.8590 Å) and O–O (1.4757 Å) bond distances of **2** are comparable to those of the Co^{III}–OO^tBu complexes (Table S2, ESI†).[1,33]

Thermal decomposition of **2** produced a Co^{III}–$(OO^tBu)(OH)$ complex, $[Co^{III}(Me_3\text{-TPADP})(OO^tBu)(OH)]^+$ (**3**), in CH_3CN at 25 °C (Fig. S2, ESI†).[34] Formation of **3** was confirmed by cold spray ionization spectrometry (CSI-MS). The CSI-MS spectrum of **3** shows a prominent signal at *m*/*z* 413.17 (calcd *m*/*z* 413.20) (Fig. S3, ESI†). Upon adding isotopically labeled $H_2{}^{18}O$ and D_2O into the solution of **3**, mass peaks at 415.21 and 414.22 corresponding to $[Co^{III}(Me_3\text{-TPADP})(OO^tBu)(^{18}OH)]^+$ (calcd *m*/*z* 415.20) and $[Co^{III}(Me_3\text{-TPADP})(OO^tBu)(OD)]^+$ (calcd *m*/*z* 414.20), respectively, were observed (Fig. S3, ESI,† the inset). These mass shifts demonstrate that **3** contains a hydroxide ligand. In a previous study, the Fe–$(OO^tBu)_2$ species was also proposed as a precursor of the Fe–(OO^tBu) species.[29] Tajima *et al.* insisted that $[Fe^{III}(TPP)(OO^tBu)_2]^-$, generated by adding an excess amount of sodium methoxide ($NaOCH_3$) and ^tBuOOH to the $[Fe^{III}(TPP)]^+$ solution, reacted with additional $NaOCH_3$, affording the formation of the $[Fe^{III}(TPP)(OO^tBu)(OCH_3)]^-$ species.[29]

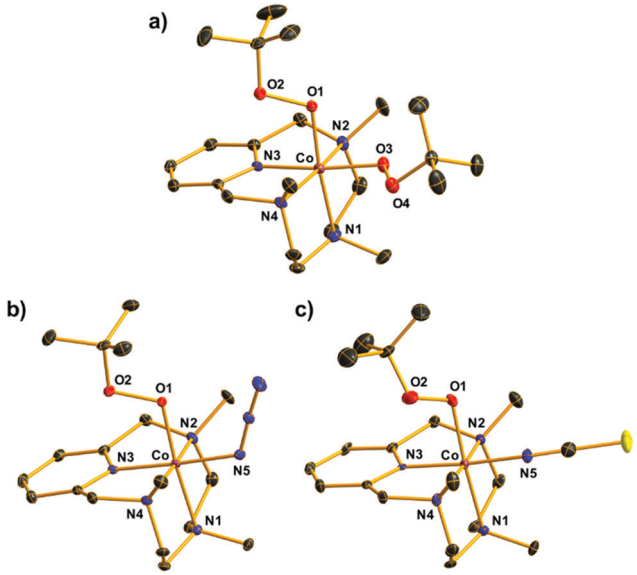

Fig. 2 ORTEP plots of the (a) Co^{III}–$(OO^tBu)_2$ complex, $[Co^{III}(Me_3\text{-TPADP})(OO^tBu)_2]^+$ (**2**), and Co^{III}–$(OO^tBu)(X)$ complexes, $[Co^{III}(Me_3\text{-TPADP})(OO^tBu)(X)]^+$ (X = (b) N_3 (**4**), (c) NCS (**5**)), with thermal ellipsoids drawn at the 30% probability level. Hydrogen atoms are omitted for clarity.

We then investigated the electrophilic and nucleophilic reactivities of **2**. The electrophilic reaction of **2** was performed by using styrene and 2,3-dimethyl-2-butene. Upon addition of substrates to the solution of **2** in CH_3CN at 10 °C, the intermediate remained intact without showing specific UV-vis spectral changes, and product analysis of these reaction solutions did not show oxidized products (Scheme 1). In contrast, the nucleophilic reactivity of **2** was observed in the oxidation of aldehydes (Scheme 1). Upon the addition of benzaldehyde to **2** in CH_3CN at 15 °C, the characteristic absorption band of **2** disappeared with a pseudo-first-order decay (Fig. 3a, the inset and Table S3, ESI†). The product analysis of the reaction solution revealed that benzoic acid (95(1)%) was produced in the oxidation of benzaldehyde (Scheme S2, ESI†). In addition, the cobalt(II)-benzoato complex, $[Co^{II}(Me_3\text{-TPADP})(C_6H_5COO)]^+$, was generated after the reaction was completed (Fig. S7, ESI† for CSI-MS analysis). The reactivity of **2** was further investigated with *para*-substituted benzaldehydes, *para*-X-Ph-CHO (X = Me, F, Cl, and CF_3) (Table S3, ESI†). The Hammett plot of the pseudo-first-order rate constants *versus* σ_p^+ gave a ρ value of 0.7(1) (Fig. 3b). The positive ρ value indicates that **2** has nucleophilic character. The reactivity of **2** was further examined by using primary (1-pentanal for 1°-CHO), secondary (2-methylbutanal for 2°-CHO), and tertiary (pivalaldehyde for 3°-CHO) aldehydes, and the observed reactivity order of 1°-CHO > 2°-CHO > 3°-CHO supports the nucleophilic character of **2** as well (Fig. S8, ESI†). Product analyses of the resulting solutions revealed that pentanoic acid (94(3)%), 2-methylbutanoic acid (94(4)%), and 2,2-dimethylpropanoic acid (94(1)%) were produced in the oxidation of 1-pentanal, 2-methylbutanal, and pivalaldehyde, respectively (Table S4, ESI†).

Upon the addition of 2-phenylpropionaldehyde (2-PPA) to **2** in CH_3CN at 25 °C under aerobic conditions, the UV-vis absorption

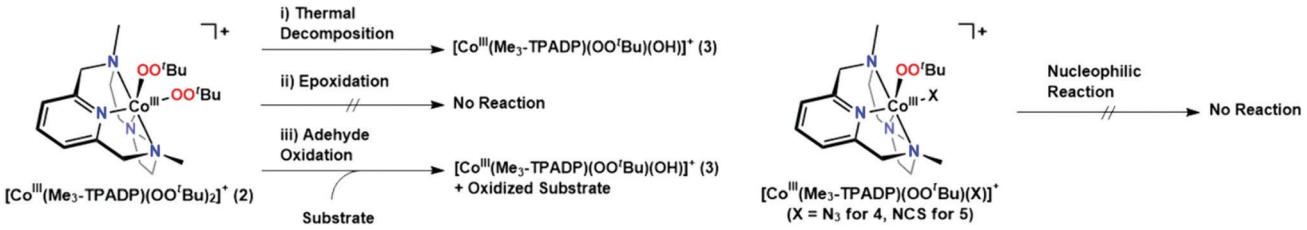

Scheme 1 Overall electrophilic and nucleophilic reactivities of **2**, **4** and **5**.

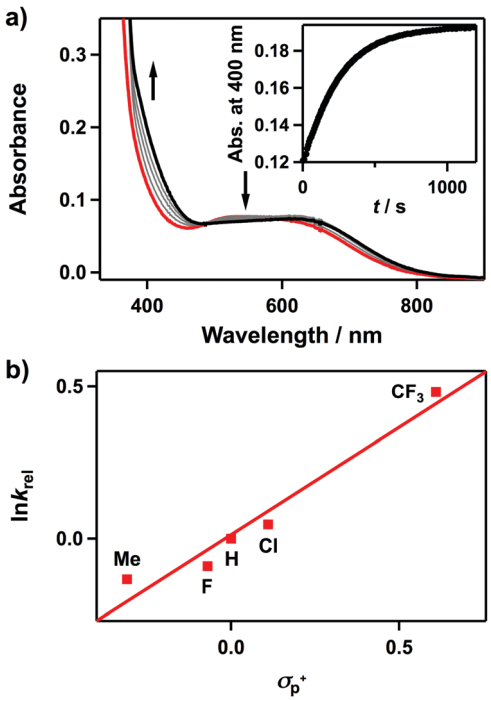

Fig. 3 Reactions of $[Co^{III}(Me_3\text{-TPADP})(OO^tBu)_2]^+$ (**2**) with benzaldehyde in CH_3CN/MeOH (v/v = 3 : 1). (a) UV-vis spectral changes of **2** (0.5 mM) upon addition of 200 equiv. of benzaldehyde at 15 °C. Inset shows the time course of the absorbance at 400 nm. (b) Hammett plot of ln k_{rel} against σ_p^+ of *para*-substituted benzaldehydes. The k_{rel} values were calculated by dividing k_{obs} of *para*-X-Ph-CHO (X = Me, F, H, Cl, and CF_3) by k_{obs} of benzaldehyde at 15 °C.

band of **2** slightly changed with isosbestic points at 390 and 452 nm, which follows a pseudo-first-order decay profile (Fig. S9, ESI†). The pseudo-first-order rate constants increased proportionally with the 2-PPA concentration, giving a second-order rate constant (k_2) of 4.1(3) × 10^{-1} M^{-1} s^{-1} at 25 °C (Fig. S10a, ESI†). After the reaction of **2** with 2-PPA, product analysis revealed that acetophenone (95(1)%) was produced as a final product. The CSI-MS spectrum of the reaction solution revealed the formation of **3** and a small amount of cobalt(II)-formato species was also detected under an inert atmosphere (Fig. S11, ESI†). The temperature dependence of the k_2 values was examined in the range of 273–298 K, where a linear Eyring plot was obtained with the activation parameters of $\Delta H^{\ddagger}$ = 11(1) kcal mol^{-1} and $\Delta S^{\ddagger}$ = −22(3) cal mol^{-1} K^{-1} (Fig. S10b, ESI†). The observed negative entropy value and the second-order kinetics suggest that the oxidation of 2-PPA by **2** is performed through a bimolecular mechanism.

Interestingly, the same reaction performed under a N_2 atmosphere gives different products. The reaction of **2** with 2-PPA under N_2 in CH_3CN at 25 °C gave a new absorption band at 480 nm (Fig. S12, ESI†). By analysing the resulting solution with CSI-MS, we found that a cobalt(II)–enolate complex, $[Co^{II}(Me_3\text{-TPADP})(OCH{=}C(Me)Ph)]^+$, was formed as a decomposed product (Fig. S13, ESI†). The product analysis of the reaction solution indicated that trace amounts of acetophenone were produced (<1%) after the reaction. When the cobalt(II)–enolate complex was exposed to O_2, a cobalt(II)–formato complex was obtained as a major product, as observed by CSI-MS (Fig. S14, ESI†). These results are very similar to Tolman's recent mechanism of the aldehyde deformylation pathway *via* a copper(II)–enolate species.[35] Based on the kinetic studies and product analyses under N_2 and O_2, the possible reaction mechanisms for 2-PPA oxidation by **2** are summarized in Scheme 2. The reaction of **2** and 2-PPA in the presence of water afforded enolate and a putative cobalt(III)–(OO^tBu) species through α-deprotonation of 2-PPA by one of the alkylperoxides of **2**. The putative cobalt(III)–(OO^tBu) species decomposed to the cobalt(II)–enolate complex under N_2. In the presence of O_2, the enolate is oxidized to acetophenone, and complex **3** is produced as a final product.

In the aldehyde oxidation, only one OO^tBu ligand in **2** was able to participate in the oxidation of 2-PPA (Scheme 1). To compare the reactivity properties of Co^{III}–(OO^tBu) and Co^{III}–$(OO^tBu)_2$ complexes, Co^{III}–(OO^tBu)(X) complexes, $[Co^{III}(Me_3\text{-TPADP})(OO^tBu)(X)]^+$ (X = N_3 for **4**, NCS for **5**), were synthesized. **4** and **5** were prepared by adding 1.1 equiv. of NaX (X = N_3, NCS) to the reaction solution of **1** in CH_3CN at 25 °C and then 5 equiv.

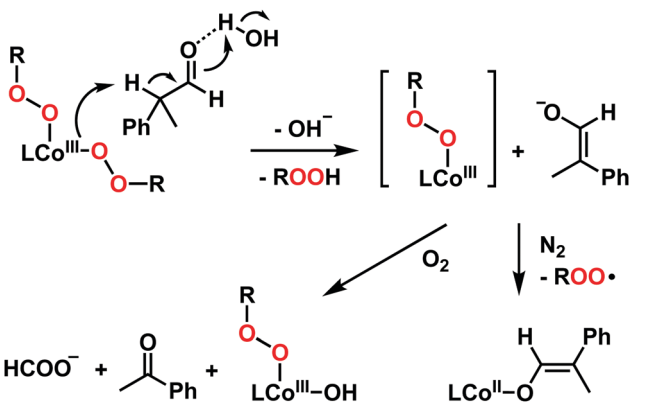

Scheme 2 Proposed reaction pathways of **2** with 2-PPA under N_2 and O_2 (L = Me_3-TPADP, R = ^{t}Bu).

of ^{t}BuOOH and 2 equiv. of TEA were added (Scheme S1, ESI†). Characterization of **4** and **5** was performed by UV-vis, ESI-MS, EPR, and ^{1}H NMR analyses (Experimental section and Fig. S15–S19, ESI†).

The single crystals of **4** and **5** revealed a similar distorted octahedral geometry to that of **2** in which one OO^{t}Bu ligand bound to the cobalt(III) center was located in the *trans* position of the amine group and the other anionic monodentate ligand, X, was located in the *trans* position of the pyridine ring (Fig. 2b and c). These data clearly indicate that the OO^{t}Bu ligand in the *trans* position of the pyridine ring in **2** was substituted with an anionic ligand in **3** and **4**. The Co–O1 bond distances (1.862(3) Å for **4**, 1.880(4) Å for **5**) and O1–O2 bond distances (1.479(4) Å for **4**, 1.430(6) Å for **5**) were within the range of those of the reported Co^{III}–OO^{t}Bu complexes and similar to those of **2** (Table S2, ESI†).[1,33]

In the reactions of **4** and **5** with 2-PPA, we could not observe any change in the UV-vis spectra. Based on the reactivity and structural comparison of **2**, **4**, and **5**, the reaction site of **2** is presumed to be the OO^{t}Bu ligand in the *trans* position of the pyridine ring. Further theoretical calculations on the detailed reaction mechanism of **2** with substrates are underway and will clarify the reaction site of **2**.

In conclusion, we have synthesized and characterized a mononuclear Co^{III}–(OO^{t}Bu)$_2$ intermediate, [Co^{III}(Me$_3$-TPADP)(OO^{t}Bu)$_2$]$^{+}$ (**2**), with various physicochemical methods including UV-vis, ESI-MS, EPR, X-ray, and NMR analyses. In the kinetic studies, under mild conditions, one of the two OO^{t}Bu ligands in **2** is capable of performing a nucleophilic reaction (*i.e.*, aldehyde oxidation). A Co^{III}–(OO^{t}Bu)(OH) complex, **3**, was generated by thermal decomposition of **2** and/or deformylation reaction of 2-PPA by **2** in the presence of O_2. Furthermore, Co^{III}–(OO^{t}Bu) complexes, [Co^{III}(Me$_3$-TPADP)(OO^{t}Bu)(X)]$^{+}$ (X = N_3 for **4**, NCS for **5**), which have a OO^{t}Bu ligand in the *trans* position of the amine group were prepared, and **4** and **5** did not undergo aldehyde oxidation.

This research was supported by the NRF (2019R1A2C2086249 and 2018R1A5A1025511) and the Ministry of Science, ICT and Future Planning (CGRC 2016M3D3A01913243) of Korea.

Conflicts of interest

The authors declare no competing financial interest.

Notes and references

1 F. A. Chavez and P. K. Mascharak, *Acc. Chem. Res.*, 2000, **33**, 539–545.
2 S. Hikichi, M. Akita and Y. Moro-Oka, *Coord. Chem. Rev.*, 2000, **198**, 61–87.
3 M. Costas, M. P. Mehn, M. P. Jensen and L. Que, Jr., *Chem. Rev.*, 2004, **104**, 939–986.
4 B. de Bruin, P. H. M. Budzelaar and A. W. Gal, *Angew. Chem., Int. Ed.*, 2004, **43**, 4142–4157.
5 S. Itoh, *Acc. Chem. Res.*, 2015, **48**, 2066–2074.
6 A. T. Fiedler and A. A. Fischer, *J. Biol. Inorg. Chem.*, 2017, **22**, 407–424.
7 J. F. Black, *J. Am. Chem. Soc.*, 1978, **100**, 527–535.
8 E. G. Kovaleva and J. D. Lipscomb, *Science*, 2007, **316**, 453–457.
9 E. Skrzypczak-Jankun, R. A. Bross, R. T. Carroll, W. R. Dunham and M. O. Funk, Jr., *J. Am. Chem. Soc.*, 2001, **123**, 10814–10820.
10 H. Komatsusuzaki, N. Sakamoto, M. Satoh, S. Hikichi, M. Akita and Y. Moro-oka, *Inorg. Chem.*, 1998, **37**, 6554–6555.
11 S. Hong, Y.-M. Lee, K.-B. Cho, M. S. Seo, D. Song, J. Yoon, R. Garcia-Serres, M. Clémancey, T. Ogura, W. Shin, J.-M. Latour and W. Nam, *Chem. Sci.*, 2014, **5**, 156–162.
12 J. A. Kovac, *Acc. Chem. Res.*, 2015, **48**, 2744–2753.
13 M. Sankaralingam, Y.-M. Lee, W. Nam and S. Fukuzumi, *Coord. Chem. Rev.*, 2018, **365**, 41–59.
14 N. Kitajima, T. Katayama, K. Fujisawa, Y. Iwata and Y. Morooka, *J. Am. Chem. Soc.*, 1993, **115**, 7872–7873.
15 J. Kim, E. Larka, E. C. Wilkinson and L. Que, Jr., *Angew. Chem., Int. Ed. Engl.*, 1995, **34**, 2048–2051.
16 M. S. Seo, T. Kamachi, T. Kouno, K. Murata, M. J. Park, K. Yoshiza-wa and W. Nam, *Angew. Chem., Int. Ed.*, 2007, **46**, 2291–2294.
17 S. Gosiewska, H. P. Permentier, A. P. Bruins, G. van Koten and R. J. M. Gebbink, *Dalton Trans.*, 2007, 3365–3368.
18 A. Kunishita, H. Ishimaru, S. Nakashima, T. Ogura and S. Itoh, *J. Am. Chem. Soc.*, 2008, **130**, 4244–4245.
19 S. Hikichi, H. Okuda, Y. Ohzu and M. Akita, *Angew. Chem., Int. Ed.*, 2009, **48**, 188–191.
20 J. Stasser, F. Namuswe, G. D. Kasper, Y. Jiang, C. M. Krest, M. T. Green, J. Penner-Hahn and D. P. Goldberg, *Inorg. Chem.*, 2010, **49**, 9178–9190.
21 T. Tano, M. Z. Ertem, S. Yamaguchi, A. Kunishita, H. Sugimoto, N. Fujieda, T. Ogura, C. J. Cramer and S. Itoh, *Dalton Trans.*, 2011, **40**, 10326–10336.
22 S. Paria, T. Ohta, Y. Morimoto, T. Ogura, H. Sugimoto, N. Fujieda, K. Goto, K. Asano, T. Suzuki and S. Itoh, *J. Am. Chem. Soc.*, 2015, **137**, 10870–10873.
23 B. Kim, D. Jeong and J. Cho, *Chem. Commun.*, 2017, **53**, 9328–9331.
24 T. Abe, Y. Morimoto, K. Mieda, H. Sugimoto, N. Fujieda, T. Ogura and S. Itoh, *J. Inorg. Biochem.*, 2017, **177**, 375–383.
25 J. Lewiński, Z. Ochal, E. Bojarski, E. Tratkiewicz, I. Justyniak and J. Lipkowski, *Angew. Chem., Int. Ed.*, 2003, **42**, 4643–4646.
26 T. Katsuki and K. B. Sharpless, *J. Am. Chem. Soc.*, 1980, **102**, 5974–5976.
27 D. E. Babushkin and E. P. Talsi, *J. Mol. Catal. A: Chem.*, 2003, **200**, 165–175.
28 M. Rivera, G. A. Caignan, A. V. Astashkin, A. M. Raitsimring, T. K. Shokhireva and F. A. Walker, *J. Am. Chem. Soc.*, 2002, **124**, 6077–6089.
29 K. Tajima, K. Tada, J. Jinno, T. Edo, H. Mano, N. Azuma and K. Makino, *Inorg. Chim. Acta*, 1997, **254**, 29–35.
30 M. P. Jensen, M. Costas, R. Y. N. Ho, J. Kaizer, A. Mairata i Payeras, E. Münck, L. Que, Jr., J.-U. Rohde and A. Stubna, *J. Am. Chem. Soc.*, 2005, **127**, 10512–10525.
31 M. P. Jensen, A. M. I. Payeras, A. T. Fiedler, M. Costas, J. Kaizer, A. Stubna, E. Münck and L. Que, Jr., *Inorg. Chem.*, 2007, **46**, 2398–2408.
32 B. Shin, K. D. Sutherlin, T. Ohta, T. Ogura, E. I. Solomon and J. Cho, *Inorg. Chem.*, 2016, **55**, 12391–12399.
33 F. A. Chavez, C. V. Nguyen, M. M. Olmstead and P. K. Mascharak, *Inorg. Chem.*, 1996, **35**, 6282–6291.
34 Interestingly, the decay of **2** was facilitated by adding excess water in **2**, and a cobalt(II)–hydroxo complex was observed as a major peak in CSI-MS (Fig. S4–S6, ESI†).
35 W. D. Bailey, N. L. Gagnon, C. E. Elwell, A. C. Cramblitt, C. J. Bouchey and W. B. Tolman, *Inorg. Chem.*, 2019, **58**, 4706–4711.

